SECOND EUROPEAN CONFERENCE ON EARTHQUAKE ENGINEERING
AND SEISMOLOGY, ISTANBUL AUG. 25-29, 2014

SOIL AND FOUNDATION PROPERTIES OF A VERTICALLY EXCITED DRILLED SHAFT

Elnaz ESMAEILZADEH SEYLABI[1], Asli KURTULUS[2], S. Farid GHAHARI [3], Fariba ABAZARSA[3], K.H. STOKOE, II[4], Chanseok JEONG[5], Ertugrul TACIROGLU[6]

ABSTRACT

Numerical and analytical approaches are used for modeling field tests that utilized a variety of excitation sources ranging from small impact hammers to large-scale mobile shakers to vertically load a drilled shaft, which induced linear to nonlinear strains in the surrounding soil at a natural site in Austin, Texas. In the field, responses of the 12-ft drilled shaft and its adjacent soil were recorded through embedded geophones. The tests were designed and performed as part of a NEES (Network for Earthquake Engineering Simulation) project aiming to evaluate the in-situ nonlinear shear stiffness of soil at depth. In the current study, field data is revisited in an attempt to (i) evaluate dynamic properties of soil and (ii) extract impedance functions of the drilled shaft. In the first part of the study, an analytical approach is used to model waves propagating away from harmonically loaded shaft in an attempt to quantify strain-dependent dynamic properties of the instrumented soil layer. In the second part of the study, numerical modeling is used to extract frequency-dependent impedance functions of the soil-shaft system. Extracted impedance functions are compared to direct impedance calculations using field data recorded at the top surface of the shaft.

INTRODUCTION

Quantification of dynamic behaviour of soil and foundation systems requires knowledge of (i) dynamic soil properties, i.e. strain-dependent stiffness and material damping properties of soil, to characterize free-field response, and (ii) impedance functions, i.e. frequency-dependent stiffness and damping properties of soil-foundation system, to characterize soil-foundation interaction. Accurate quantification of these is considered as a critical issue in designing earthquake-resistant structures.

A number of field and laboratory techniques have been developed over the last decades to measure the dynamic properties of soils (Kramer, 1996). The ability of laboratory tests to provide accurate measurements of dynamic soil properties is affected by several factors, such as sample disturbance, specimen size, loading conditions, and reproduction of actual field conditions. At present, there is no validated test method for determining strain-dependent dynamic soil properties in the field. The need for in-situ measurements of soil properties at a wide range of strains has led the geotechnical research team at The University of Texas at Austin to design and perform a series of field tests, which were successfully applied at a natural soil test site in Austin, Texas (Kurtulus and Stokoe, 2008). The tests

[1] PhD Candidate, University of California at Los Angeles, USA, esmaeilzadeh@ucla.edu
[2] Assoc. Prof., Ozyegin University, Istanbul, Turkey, asli.kurtulus@ozyegin.edu.tr
[3] Postdoctoral Researcher, University of California at Los Angeles, USA, ghahari@gmail.com
[4] Prof., The University of Texas at Austin, USA, k.stokoe@mail.utexas.edu
[5] Assis. Prof., The Catholic University of America, USA, jeong@cua.edu
[6] Prof., University of California at Los Angeles, USA, etacir@ucla.edu

were designed and performed as part of a NEES (Network for Earthquake Engineering Simulation) project aiming to evaluate the in-situ nonlinear shear stiffness of soil at depth. The test results proved that by using a vertically excited drilled shaft as a shear wave generator it was possible to evaluate linear to nonlinear (from 0.0001% to 0.05% strain) in-situ shear stiffness of a silty soil at depth. The in-situ evaluated shear modulus reduction curve fits the expected trends and the normalized curve was in agreement with the laboratory curve from an intact specimen as well as empirical curves (Kurtulus and Stokoe, 2008).

Several number of studies have been carried out in the last decades to compute the impedance functions for different types of soil-foundation systems. In these efforts, various modelling techniques were employed, including analytical, semi-analytical, and numerical approaches (e.g. Dobry and Gazetas, 1986; Pais and Kausel, 1988). Nearly all of the available impedance functions are for relatively simple soil profiles and rigid foundations. Moreover, very few, and only for shallow foundations, field validation of impedance functions exists in literature (Crouse and Luco, 1990; Tileylioglu et al., 2011). Therefore, field verification is crucial to validate the theoretically computed impedance functions, especially for deep foundations. The need for a robust method that can yield impedance functions for any soil profile and for foundations with different types and shapes has led the research team at University of California at Los Angeles to develop a procedure for numerically extracting impedance functions from high-fidelity finite element models (Jeong et.al, 2013).

In this study, parts of this field data is revisited to evaluate dynamic characteristics of soil and foundation system. The first part of this study deals with evaluation of dynamic soil properties from the NEES field data using an existing analytical approach. The second part deals with evaluation of impedance functions of the soil-shaft system via extending a tool recently developed by Jeong et al. (2013) to compute the impedance functions of axisymmetric problems in the frequency domain. The validation of these theoretical results against field measurements are provided. In the next sections, following a brief description of field tests, details of both parts of study and the results obtained are presented.

FIELD TESTS

The field tests involved axial loading of the 12-ft long concrete drilled shaft using a variety of energy sources that allow loading the drilled shaft with successively larger forces. Three types of vertical dynamic sources were employed successively to load the shaft in stages. The dynamic sources were: (1) hand-held instrumented hammers which were used to generate small impulses with varying frequency contents, (2) ‘Thumper’ (smaller capacity NEES vibroseis shaker), and (3) ‘TRex’, (larger capacity NEES vibroseis shaker).

The 12-ft long and 15-in. diameter shaft was reinforced with a steel cage and was constructed using concrete having a compressive strength of approximately 4800 psi. Prior to construction, the rebar cage of the shaft was instrumented with vertical velocity transducers (also called geophones or sensors) at two depths within the shaft. Based on modal hammer tests performed in the field and laboratory tests conducted on concrete cylinder samples, the shaft had an unconstrained compression wave velocity of about 12700 fps and a unit weight of around 130 pcf.

The shaft was extended about 6 in. above the ground surface to allow the loading system to be mounted. Three or more small-diameter (as small as 6 in.) boreholes were installed in the soil adjacent to the shaft at successively larger radial distances from the shaft. The distance from the edge of the drilled shaft to the nearest borehole was as close as 3 to 6 in. The boreholes were instrumented with geophones at two depths (approximately 12 in. apart). Shear waves propagating away from the mid-depth of the shaft were measured using vertically oriented geophones that were embedded in the soil prior to testing. Each sensor was 1.5 in. in diameter and 2.3 in. in length and consisted of a single, 14 Hz geophone oriented in the vertical direction. The unit weight of the sensors was approximately 135 pcf while the unit weight of surrounding soil at the time of testing was around 110 pcf. A schematic illustration of the field test configuration is shown in Figure 1a and b. The exact locations of the sensors were obtained by excavating the test area after completion of all field tests (Figure 1c).

In the first stage of dynamic testing, instrumented hand-held hammers were used to perform tests in the linear strain range by generating small impacts at the top of the shaft. During these tests a 14-Hz geophone was also attached to the top surface of the shaft. The impact tests provided measurements that could be compared to lowest amplitude steady-state tests using smaller vibroseis truck as sources. In the next stages, 'Thumper' and then 'TRex' were mounted on top of the shaft and operated in the vertical direction to apply sinusoidal loading at a selected frequency for a selected number of cycles. Dynamic loads from each vibroseis truck were increased successively to conduct a staged testing. The sequence of dynamic loading applied using vibroseis shakers is shown in Table 1. A static vertical hold-down force load had to be exerted on the shaft in order to apply dynamic loads. The field testing arrangement is shown in Figure 2. A sampling rate of 200 ksamples/s was used to simultaneously record the response of all embedded geophones to the applied loading.

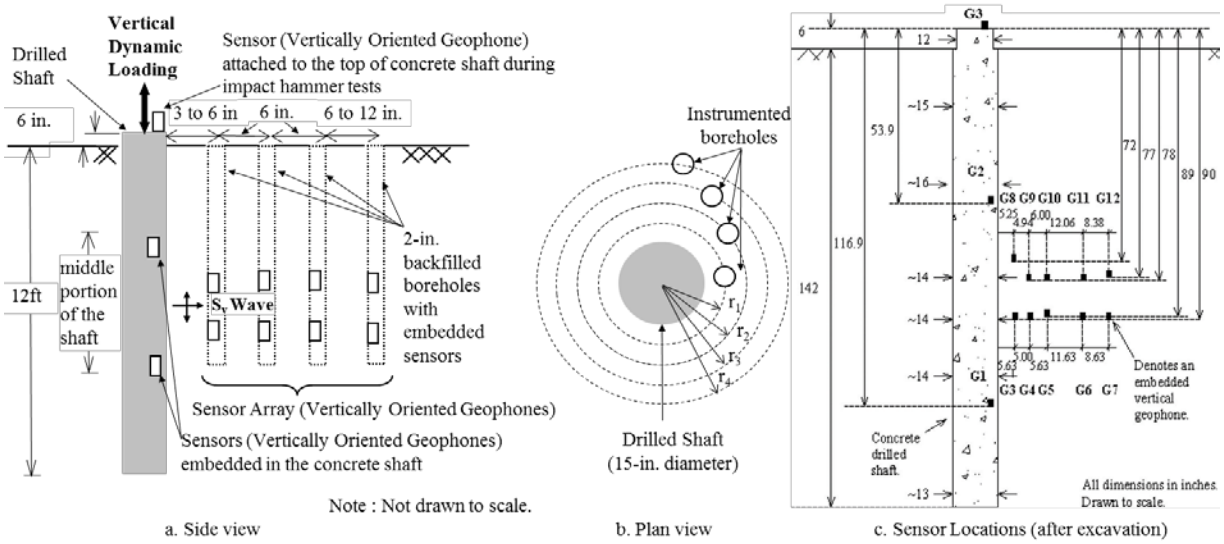

Figure 1. Schematic illustration of field test configuration

Figure 2. Dynamic testing using a variety of energy sources

Table 1. Sequence of loading steps applied to the shaft using vibroseis shakers

Test No.	Source	Static Load (lbs.)	Dynamic Load (lbs.)	Loading Type
1	Thumper	2000	180	15 cycles at 55 Hz
2	Thumper	2000	240	15 cycles at 55 Hz
3	Thumper	2000	360	15 cycles at 55 Hz
4	Thumper	2000	480	15 cycles at 55 Hz
5	Thumper	2000	600	15 cycles at 55 Hz
6	Thumper	2000	720	15 cycles at 55 Hz
7	Thumper	2000	840	15 cycles at 55 Hz
8	Thumper	2000	960	15 cycles at 55 Hz

Table 1 continued

9	Thumper	2000	1080	15 cycles at 55 Hz
10	Thumper	2000	1200	15 cycles at 55 Hz
11	Thumper	4000	1440	15 cycles at 55 Hz
12	Thumper	4000	1800	15 cycles at 55 Hz
13	Thumper	4000	2400	15 cycles at 55 Hz
14	Thumper	8000	3600	15 cycles at 55 Hz
15	Thumper	8000	6000	15 cycles at 55 Hz
16	T-Rex	20000	20000	10 cycles at 55 Hz
17	T-Rex	50000	35000	10 cycles at 55 Hz

WAVE PROPAGATION ANALYSIS

Wave Equation

Detailed site characterization studies that were performed at the field test site (Kurtulus, 2006) showed that the site is basically composed of three soil layers overlying engineering bedrock as illustrated in Figure 3. Modal hammer tests performed in the field prior to staged dynamic testing using vibroseis shaker revealed that the first mode resonance frequency of the shaft was approximately 500 Hz, which is far from the sinusoidal loading frequency (i.e. 55 Hz, Table 1) therefore the shaft can be assumed as a rigid source.

The main assumptions considered here are:

- An equivalent soil layer with thickness equal to the total thickness of the layers is used to model the problem.
- The equivalent soil layer is homogenous and isotropic.
- Soil is linear and elastic (for tests with large dynamic loading, soil is equivalent linear).
- Radial displacements are negligibly small.
- Material damping is hysteretic and frequency-independent.
- Material damping associated with both volumetric and shear strains are identical.
- The shaft is assumed to be extending to the rigid bedrock (which is logical assumption considering the location of the geophones).

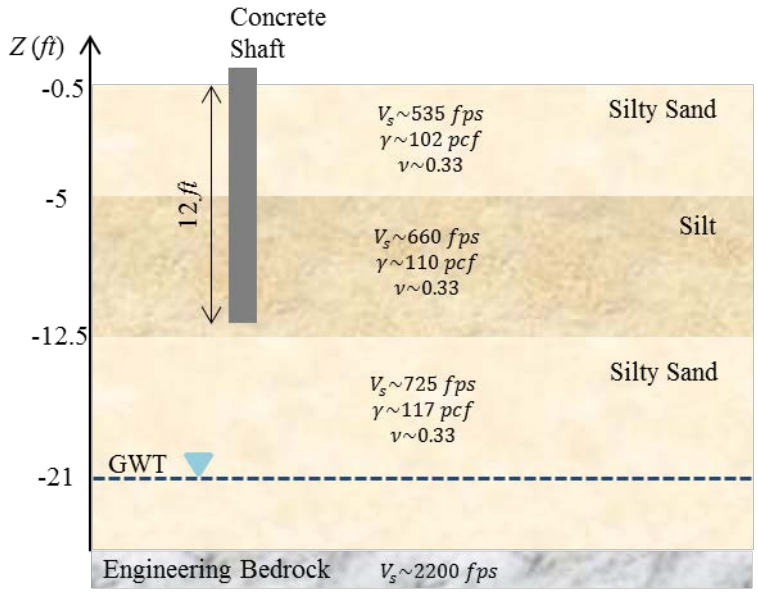

Figure 3. Schematic representation of soil profile at the test site

It is well-known that the vertical deformation of soil element under harmonic vibration of the shaft can be expressed as modal summation as (Nogami and Novak, 1976)

$$w(r,z,t) = e^{i\omega_0 t}\sum_{n=1}^{\infty} A_n K_0(q_n r)\, sin(h_n z) \tag{1}$$

where A_n are modal constants and $w(r,z,t)$ denotes soil displcament at depth z, time t, and radial distance from the shaft r. ω_0 is the excitation frequency and K_0 is the modified Bessel functions of zero-order and second kind (Abramowitz and Stegun, 1964). h_n is calculated as

$$h_n = \frac{\pi}{2H}(2n-1) \qquad \text{for} \quad n = 1, 2, 3, \ldots \tag{2}$$

in which H is the thickness of the equivalent soil layer. For each mode, parameter q_n is defined using excitation frequency (ω_0), soil shear wave velocity (V_s), soil material damping (ξ), and dimensionless parameter $\eta = \sqrt{\frac{2}{1-\nu}}$ (Mylonakis, 2001) as follows

$${q_n}^2 = \frac{\eta^2(1+2i\xi){h_n}^2 - \left(\frac{\omega_0}{V_s}\right)^2}{(1+2i\xi)} \tag{3}$$

Natural frequency of the soil layer can be estimated by solving equation $q_n = 0$; that is, the frequency of excitation which causes largest response (resonance). Accordingly, undamped natural frequencies of the soil layer are obtained as

$$\omega_n = \eta\, V_s \frac{\pi}{2H}(2n-1) \qquad \text{for} \quad n = 1, 2, 3, \ldots \tag{4}$$

According to the available information about the soil layers (Kurtulus 2006), soil layer in which soil displacement is recorded (Layer 2 in Figure 3) has an inital shear wave velocity around 660fps. So, we expect this layer to have the largest contribution to the overall response. By inserting this value into Eq. (4) and assuming a frequency equal to $\omega = 346\ \mathrm{rad/s}$ as loading frequency, we have $n = \frac{H\omega}{\pi\eta\, V_s} + \frac{1}{2} \cong 4$. In other words, by applying a harmonic loading with frequency $\omega_0 = 346\ \mathrm{rad/s}$, the soil deformation will approximately exhibit the relationship

$$w(r,z,t) \cong A_4 K_0(q_4 r)\, sin(h_4 z) e^{i\omega_0 t} \tag{5}$$

which can be written in polar form as

$$w(r,z,t) \cong A_4 sin(h_4 z)|K_0(q_4 r)|e^{i\varphi(q_4 r)}\, e^{i\omega_0 t} \tag{6}$$

Note that A_4 is constant for all depths and distances. Also, the term $sin(h_4 z)$ is constant for a specified depth.

Estimation of Shear-Wave Velocity and Damping Ratio

The wave equation shown in Eq. (6) indicates that displacement time-histories recorded at two points at the same depth will have the same shape but will exhibit different maximum amplitudes and phases. If we assume a distance Δr between two points at the same depth, then we can write

$$w(r_j, t) = \left|K_0(q_4 r_j)\right| e^{i[\omega t + \varphi(q_4 r_j)]}$$

$$= w\left(r_i, t + \frac{\varphi(q_4 r_j) - \varphi(q_4 r_i)}{\omega}\right) \frac{\left|K_0(q_4 r_j)\right|}{|K_0(q_4 r_i)|} \tag{7}$$

That is, $w(r_j, t)$ is a shifted and amplitude modulated version of $w(r_i, t)$. The constant modification factor is $\frac{|K_0(q_4 r_j)|}{|K_0(q_4 r_i)|}$ and the time-lag is $\tau = \frac{\varphi(q_4 r_j) - \varphi(q_4 r_i)}{\omega}$. We can then calculate the cross-correlation (Bendat and Piersol, 1980) between two signals recorded at points i and j at different time lags, denoted as $c_{ij}(\tau)$. This cross-correlation will have a maximum at $\tau = \frac{\varphi(q_4 r_j) - \varphi(q_4 r_i)}{\omega}$, and its value at this lag will be

$$c_{ij}\left(\frac{\varphi(q_4 r_j) - \varphi(q_4 r_i)}{\omega}\right) = \frac{\left|K_0(q_4 r_j)\right|}{|K_0(q_4 r_i)|}\, c_{ii}(0) \tag{8}$$

where $c_{ii}(0)$ is the auto-correlation of signal recorded at point i. The shear wave velocity between two points is calculated through the identified time delay as

$$V_{s_{ij}} = \Delta r / \tau \tag{9}$$

Then, material damping is estimated by minimizing both of the following residuals

$$R_1 = \left| c_{ij}\left(\frac{\varphi(q_4 r_j) - \varphi(q_4 r_i)}{\omega}\right) - \frac{\left|K_0(q_4 r_j)\right|}{|K_0(q_4 r_i)|}\, c_{ii}(0) \right| \tag{10}$$

$$R_2 = \left| \frac{\varphi(q_4 r_j) - \varphi(q_4 r_i)}{\omega} - \tau \right| \tag{11}$$

Results

Herein, we only present results for the dynamic tests performed using 'Thumper' as introduced in Table 1 and only for the geophones G1, G2, G3, G4, and G5. Results obtained from the last two tests, i.e. those performed using 'TRex', are excluded here, because they do not follow the usual trend. As an example, the displacement time-histories at these geophones are shown in Figure 4 for Test No. 1. Shear wave velocities between two geophones G3-G4, G4-G5, and G3-G5 are estimated using Eq. (10) and presented in Table 2. Damping ratios are also estimated through the minimization process defined using Eqs. (11) and (12) and presented in Table 3.

Figure 5 displays the variation of shear wave velocity and damping ratio with respect to dynamic loading amplitude. As it can be seen in Figure5a, shear wave velocity does not change significantly till Test No. 10 (1200 lbs) and then decreases by increasing loading amplitude. As shear wave velocity is

obtained from time delay, the results obtained from largest radial distance would be more reliable, i.e., G3-G5. In Figure5b, the variation of the identified material damping ratio with respect to loading amplitude is shown. As it is expected, by increasing amplitude, damping ratio increases; however, the variation is more significant after Test No. 6. As the damping ratio estimation is very sensitive to the level of vibration, the values obtained from closest sensors to the shaft, i.e., G3-G4, are more reliable.

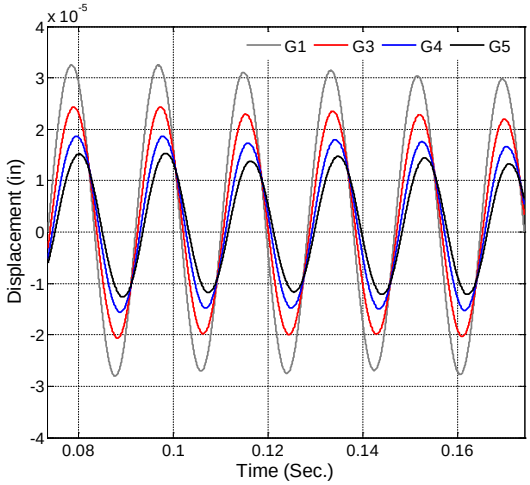

Figure 4. Displacement time histories recorded at Geophones No.1 and No.3 to 5 during Test No. 1.

Table 2. Shear wave velocity (*fps*) identified from correlation analysis

Test No.	1	2	3	4	5	6	7	8	9	10	11	12	13	14	15
G3-G4	766	766	766	773	773	773	766	773	766	766	725	712	677	611	557
G4-G5	823	809	809	816	809	809	809	809	802	802	750	744	704	683	658
G3-G5	795	788	788	792	792	792	788	788	788	788	741	726	691	647	607

Table 3. Material damping ratio (%) identified from wave equation

Test No.	1	2	3	4	5	6	7	8	9	10	11	12	13	14	15
G3-G4	11.0	12.0	12.4	12.4	12.3	12.4	12.9	13.0	13.7	13.6	15.2	15.8	15.5	14.7	15.6
G4-G5	9.2	9.9	10.1	10.2	9.8	10.0	10.2	10.4	11.3	10.7	11.1	11.2	11.0	9.1	7.62
G3-G5	10.1	10.9	11.2	11.2	11.0	11.2	11.4	11.6	12.5	12.2	13.1	13.3	12.9	11.8	11.5

As conditions of the field test may not satisfy all assumptions considered in theory, material damping ratios identified by the formula may be questionable. For this reason, we simply compare the value of $c_{ij}\left(\frac{\varphi(q_4 r_j)-\varphi(q_4 r_i)}{\omega}\right)/c_{ii}(0)$ to distinguish radiation damping and material damping. Figure 6 presents inverse of these values as "amplification factors" between each two sensors. To be able to present all curves in the same plot, we have normalized them to their minimum value, which is attributed to the minimum dynamic loading. If system does not have any material damping, it is expected all these curves to be constant with value of 1, because radiation damping is theoretically same in all tests. However, the figure shows that by increasing loading amplitude, all curves increase from 1 because of the presence of material damping. It is trivial that energy is more dissipated between two sensors which

have largest distance. So, the amplification factors for G1/G5 and G1/G3 are largest. Also, as it can be seen, between G3/G4 and G4/G5, G3/G4 has higher slope, although distance between them are smaller than distance between G4 and G5. The reason is that material damping ratio decreases by decreasing amplitude of vibration.

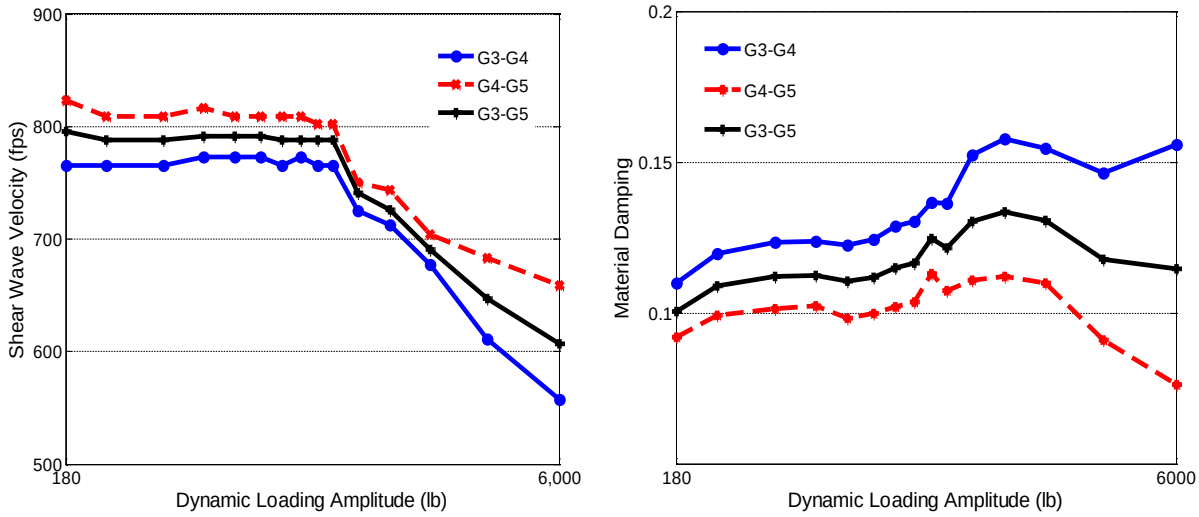

(a) (b)

Figure 5. Variations of a) shear wave velocity, and b) material damping ratio of soil with dynamic loading amplitude

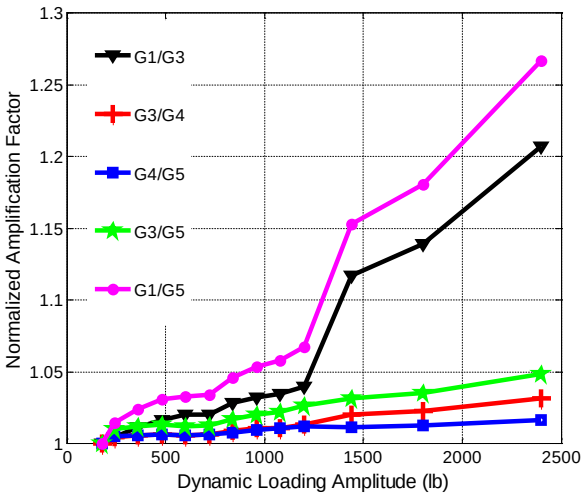

Figure 6. Effects of dynamic loading amplitude on normalized amplification factors

Finally, we compare displacement time histories which are predicted/reconstructed by the analytical approach and those recorded during field tests. As an example, Figure 7 shows this comparison for one test, Test No 14 corresponding to 3600 *lbs* dynamic loading. We have matched analytical and recorded signals at G3 in both amplitude and phase and then predicted responses at two other geophones, G4 and G5, through analytical formula and identified properties reported in Tables 2 and 3. As it can be seen, almost perfect match is observed at steady-state parts of recorded signals. That confirms the accuracy of the identified shear wave velocities and damping ratios.

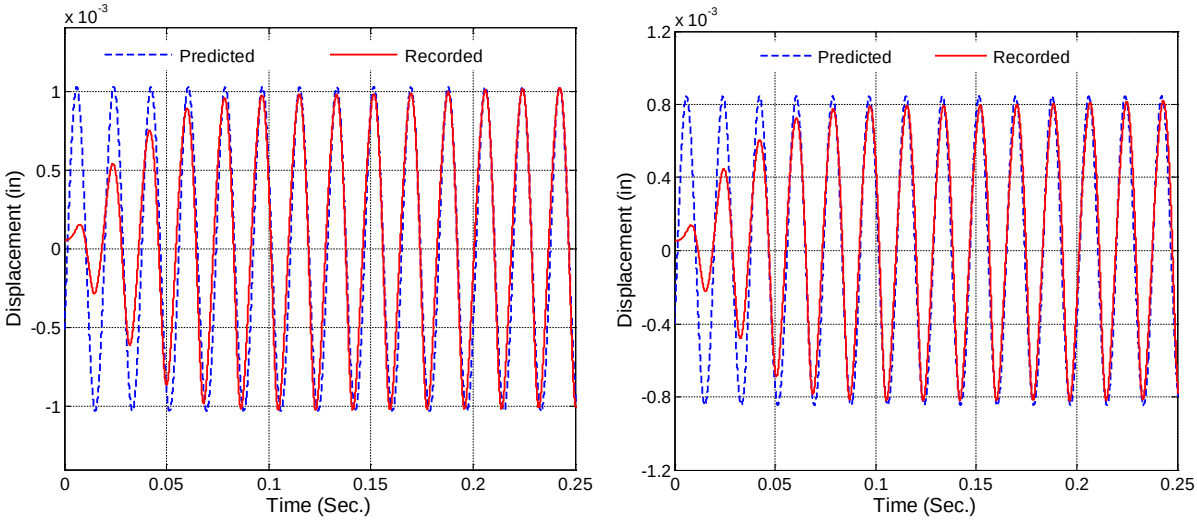

Figure 7. Comparison between reconstructed and recorded signals at (left) G4 and (right) G5 during Test No. 14

NUMERICAL ANALYSIS

Finite-Element Modeling

The shaft is loaded vertically in the impact hammer test and, as mentioned before, the surrounding soil layering is assumed to be horizontal. Therefore, it is a plausible assumption to consider the test configuration as an axisymmetric elastodynamics problem. In order to solve the problem numerically, finite element method is used to discretize the soil medium and the shaft. Moreover, the computational domain is truncated with Perfectly-Matched-Layers (PMLs) to take the effects of semi-infinite soil into account accurately and efficiently. Ideally, PMLs can absorb both propagating and evanescent waves perfectly irrespective of their angle of incidence upon the interface of the regular domain and the PML. Kucukcoban and Kallivokas (2010) proposed mixed PMLs for transient wave propagation in axisymmetric elastic media, in which both displacement and stress history are considered as primal fields in both the regular computational domain and the PML.

In this study, the idea of hybrid PMLs exists for transient simulation of plain strain problems (Kucukcoban and Kallivokas, 2013) is extended to axisymmetric problems, in which only the displacement is considered as a primal field in the whole domain while the stress history field is defined only within the PML. Moreover, the recently developed time domain approach of numerically extracting the impedance functions of soil-foundation systems (Jeong et al., 2013) is extended to the frequency domain to make the methodology not only input-independent but also viable to incorporate spatially varying low-strain material damping into the analysis.

The final semi-discrete system of wave equations is as follows:

$$\mathbf{M}\dddot{\mathbf{d}}(t) + \mathbf{C}\ddot{\mathbf{d}}(t) + \mathbf{K}\dot{\mathbf{d}}(t) + \mathbf{G}\mathbf{d}(t) = \dot{\mathbf{f}}(t) \tag{13}$$

Here, ($\dot{}$, $\ddot{}$, $\dddot{}$) are first, second and third derivative of the subtended variable with respect to time t. **M**, **C**, **K** and **G** are system matrices[7]. **d** and **f** are semi-discrete primal field and external force vectors defined as

$$\mathbf{d}^T = [\mathbf{u}_r^T \quad \mathbf{u}_z^T \quad \mathbf{S}_{rr}^T \quad \mathbf{S}_{\theta\theta}^T \quad S_{zz}^T \quad \mathbf{S}_{rz}^T] \tag{14}$$

$$\mathbf{f}^T = [\mathbf{f}_r^T \quad \mathbf{f}_z^T \quad \mathbf{0} \quad \mathbf{0} \quad \mathbf{0} \quad \mathbf{0}] \tag{15}$$

[7] Details are system matrices are not provided here because of page limitations. One may find more details on mixed formulation in Kucukcoban ad Kallivokas (2010). The extension of this method to hybrid formulation implemented here is straightforward.

where $\mathbf{u}_r$ and $\mathbf{u}_z$ are radial (horizontal) and vertical displacement vectors, respectively. $\mathbf{S}_{ij}$ $(i,j = r,z,\theta)$ are nonzero components of axisymmetric stress history vectors. $\mathbf{f}_r$ and $\mathbf{f}_z$ are radial and vertical prescribed force vectors within the regular domain.

Evaluation of Impedance Functions

In order to extract the impedance functions for a rigid interface (top-surface of the shaft in this study), it is assumed that the known displacement $u_0 e^{i\omega t}$ is applied along the surface of interest. Substituting this in equation (13) and factoring out $e^{i\omega t}$ results in:

$$\left[(i\omega)^3\mathbf{M} + (i\omega)^2\mathbf{C} + (i\omega)\mathbf{K} + \mathbf{G}\right]\hat{\mathbf{d}}(\omega) = (i\omega)\hat{\mathbf{f}}(\omega) \tag{16}$$

where $(\widehat{\ })$ is the complex-valued notation of the subtended variable in frequency domain. Solving (16) for radial frequency ω, summing up the resulting force vector along the surface of interest and dividing that by the imposed known displacement results in the impedance function $S(\omega)$. In other words:

$$S(\omega) = \frac{\sum_{j=1}^{n} \hat{f}_j(\omega)}{u_0} \tag{17}$$

where n is the number of discretized nodes along the surface of interest.

In this study, we used our numerical tool to extract the vertical impedance function of a concrete shaft embedded in a horizontally layered soil. Properties of the concrete and soil layers used in the numerical modeling are shown in Figure 3. Two cases are considered: (i) heterogeneous soil with provided layering information, and (ii) homogeneous soil with properties of the first layer. The numerically calculated impedance function is normalized as:

$$S_V(\omega) = \mu_1 D[K_V(\omega) + ia_0 C_V(\omega)] \tag{18}$$

Here, μ_1 is the shear modulus of the soil in the first layer, D is the diameter of the shaft, and K_V and C_V are frequency dependent stiffness and damping, respectively. $a_0 = \omega D/V_{s1}$ is the non-dimensional frequency and V_{s1} is the shear wave velocity in the first layer.

It is well known that damping in soil consists of material and radiation damping. In low-strain range of behavior, the first component is usually assumed to have frequency independent nature while the second component is assumed to have viscously frequency dependent nature. One major problem in characterization of dynamic soil properties by means of field experiments is the uncertainty involved in the evaluation of soil material damping, even at low-strain ranges (Redpath et al., 1982). This is mainly due to the difficulty of quantifying the radiation damping part of the response.

Results

In this study, while PML is used for accurate replication of radiation damping in semi-infinite soil domain, the Correspondence principle is used to quantify the amount of low-stain material damping ξ. In this case, the vertical impedance of the shaft-soil system can be formulated as:

$$S_V^*(\omega) = (1 + 2i\xi)S_V(\omega) = \mu_1 D[K_V^*(\omega) + ia_0 C_V^*(\omega)] \tag{19}$$

In order to obtain the correct value of low-strain material damping, the impact hammer test data is used to compute the shaft impedance function as well. To this end, Fourier transform is used to transform the recorded impact input signal and top-surface velocity of the shaft in time to the frequency domain. Then, the displacement of the top-surface is obtained via dividing the resulting velocity by $i\omega$. The ratio of the impact input to this displacement gives the impedance function (named field impedance hereafter) of the field data.

Figure 8 shows the amplitude and phase of the input signal. As seen, the test has rich frequency contents for non-dimensional frequency ranging from 0.1 to 1.2. Figure 9 shows the normalized real and

imaginary parts (stiffness and damping) of the numerically computed impedance function for layered and homogeneous soil cases versus the field impedance values. Two values of material damping $\xi = 0$ and $\xi = 0.05$ are considered. It should be noted that different values of ξ are tested to obtain the best value of 5%. As seen, the field and numerical impedances are in a very good agreement. For lower ranges of frequency the field impedance (especially the stiffness component) lays along the impedance of the shaft embedded in the layered soil with $\xi = 0.05$. As frequency increases, the values of field impedance gradually shift toward the impedance of the shaft embedded in the homogenous soil with $\xi = 0.05$.

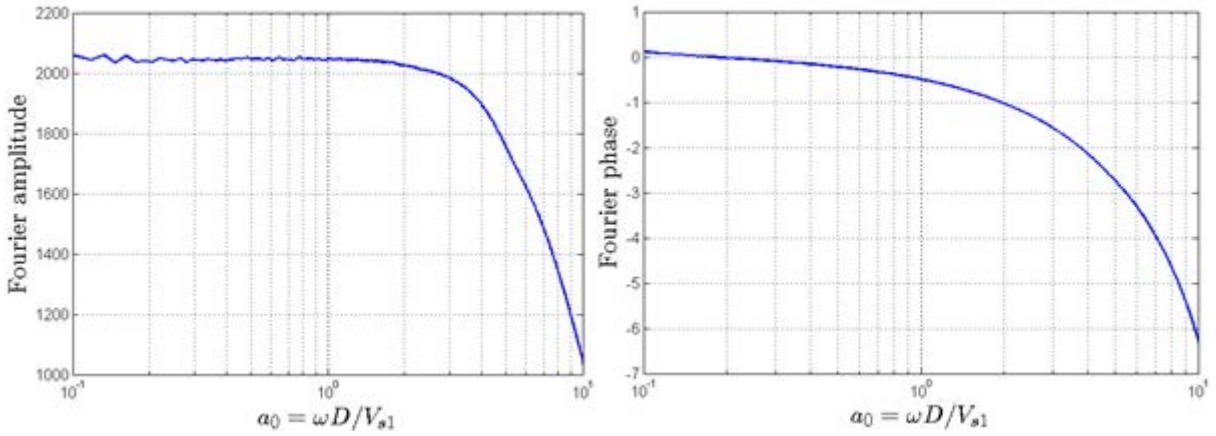

Figure 8. Fourier amplitude and phase of the input signal for the impact hammer test

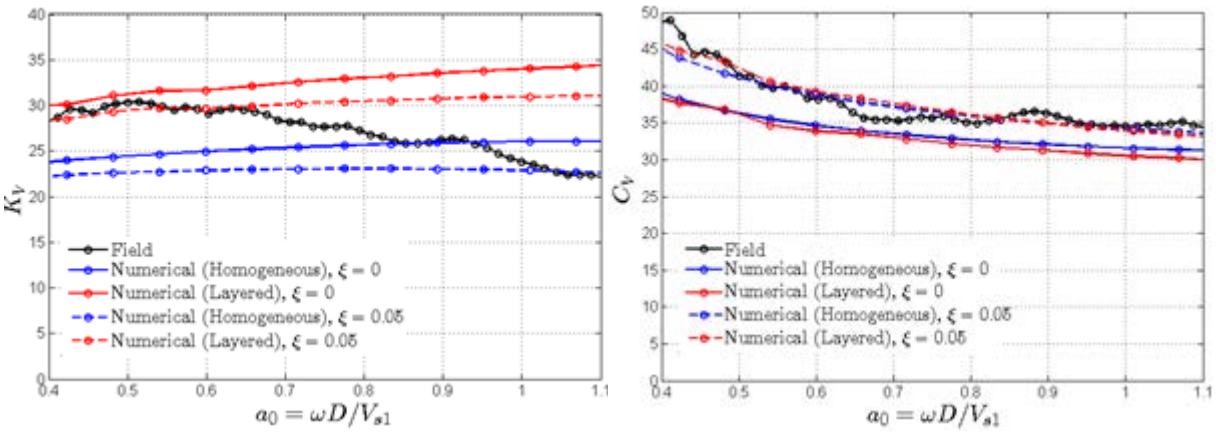

Figure 9. Comparison of numerical and field results of the stiffness and damping of the non-rigid shaft embedded in an elastic soil

CONCLUSIONS

The analytically derived wave equation has been successful to predict the measured response of soil. The variations of shear wave velocity and material damping ratio with increasing levels of dynamic excitation as determined from the analytical study show the expected trends (i.e decreasing shear wave velocity and increasing material damping ratio with increasing excitation). However, the damping ratio values that are evaluated through an optimization process are found to be considerably higher than expected. The investigation of trends in amplitude dependency of damping ratio with respect to same set of sensors indicate that the obtained values do not involve radiation damping term. Moreover, the perfect fit between the measured and reconstructed waveforms confirms the accuracy of identified soil properties. The unusually high values of material damping ratios can possibly be associated with near-source effects. However, more investigations are needed in this regard.

The numerical approach is developed to extract vertical impedances of a shaft embedded in heterogeneous elastic soil medium via solving an axisymmetric PML-truncated elastodynamics problem in the frequency domain. The methodology is validated via numerical simulation of the field test condition, and comparing the numerically extracted impedances against those derived from the impact hammer test. The developed methodology make it also possible to quantify the amount of low-strain material damping more realistically while PML takes the effects of radiation damping into account. The work is under progress to extract dynamic soil properties, i.e., strain-dependent equivalent linear shear modulus and material damping ratio, using our numerical tool presented here that will also provide more insight on the extend of accuracy of the presented analytic method in predicting strain-dependent soil properties.

REFERENCES

Abramowitz M, and Stegun IA (1964) Handbook of Mathematical Functions, National Bureau of Standards, Applied Math.

Bendat JS and Piersol AG (1980) Engineering applications of correlation and spectral analysis, John Wiley & Sons Inc., New York.

Crouse CB, Hushmand B, Luco J and Wong H (1990) "Foundation impedance functions: Theory versus experiment," *Journal of Geotechnical Engineering*, 116(3):432–449.

Dobry R and Gazetas G (1986) "Dynamic response of arbitrary shaped foundations," *Journal of Geotechnical Engineering*, 112:109–135.

Jeong C, Esmaeilzadeh Seylabi E and Taciroglu E (2013) "A Time-Domain substructuring method for dynamic soil-structure-interaction analysis of arbitrarily shaped foundation systems on heterogeneous media," *Computing in Civil Engineering*, 346-353.

Kramer SL (1996) Geotechnical earthquake engineering. Practice Hall, New Jersey, 653pp.

Kucukcoban S and Kallivokas LF (2010) "A mixed perfectly-matched-layer for transient wave simulations in axisymmetric elastic media" *Computer Modeling in Engineering and Science*, 64 (2): 109-144.

Kucukcoban S and Kallivokas LF (2013) "A symmetric hybrid formulation for transient wave simulations in PML-truncated heterogeneous media" *Wave Motion*. 50(1):57-79.

Kurtulus A (2006) "Field measurements of the linear and nonlinear shear moduli of soils using drilled shafts as dynamic cylindrical sources," Ph.D. thesis, Univ. of Texas at Austin, Austin, Tex.

Kurtulus A and Stokoe KH (2008) "In situ measurement of nonlinear shear modulus of silty soil," *Journal of Geotechnical and Geoenvironmental Engineering*, ASCE, 134(10):1531-1540.

Mylonakis G (2001) "Winkler modulus for axially loaded piles," *Geotechnique*, 51(5):455-461.

Nogami T and Novak M (1976) "Soil-pile interaction in vertical vibration," *Earthquake Engineering & Structural Dynamics*, 4(3):277-293.

Pais A, Kausel E (1988) "Approximate formulas for dynamic stiffnesses of rigid foundations," *Soil Dynamics and Earthquake Engineering*; 7(4):213 – 227.

Redpath BB, Edwards RB, Hale RJ and Kintzer FZ (1982) "Development of field techniques to measure damping values for near-surface rocks and soils," Report, URS/John A. Blume and Associates, San Francisco, 120 pp.

Tileylioglu S, Stewart JP, Nigbor RL (2011) "Dynamic stiffness and damping of a shallow foundation from forced vibration of a field test structure," *ASCE Journal of Geotechnical and Geoenvironmental Engineering*; 137(4):344–353